

1 Stratification and Mixed Layer Depth around 2 Iceland: Characterization and inter-annual 3 variability

4 Angel Ruiz-Angulo ^{1*}, Esther Portela ², Charly de Marez¹, Andreas Macrander³,
5 Sólveig Rósa Ólafsdóttir³, Thomas Meunier ⁴, Steingrímur Jónsson ^{3,5}, and M. Dolores
6 Pérez-Hernández ⁶

7 ¹Earth Science Institute, University of Iceland, 101 Reykjavik, Iceland

8 ²Univ. Brest, Laboratoire d'Océanographie Physique et Spatiale, CNRS, IRD, Ifremer, Plouzané, France

9 ³Hafrannsóknastofnun / Marine and Freshwater Research Institute, Hafnarfjörður, Iceland,

10 ⁴Woods Hole Oceanographic Institution, Woods Hole MA, USA

11 ⁵University of Akureyri, Akureyri, Iceland

12 ⁶Unidad océano y clima, Instituto de Oceanografía y Cambio Global, IOCAG, Universidad de Las Palmas de Gran Canaria,
13 ULPGC, Unidad Asociada ULPGC-CSIC, Las Palmas de Gran Canaria, Spain

14 *Correspondence to:* Angel Ruiz-Angulo (angel@hi.is)

15 ABSTRACT

16 The ocean around Iceland is a key region where major water masses and currents interact, influencing the global ocean
17 circulation. Here, we analyze 29 years (1990-2019) of quarterly hydrographic section data collected around Iceland. The
18 hydrographic properties around Iceland show important spatial variability. Based on temperature, salinity, and stratification
19 structure, we classified the Icelandic waters in three distinct regions: the south, the north and northeast regions. The warm
20 and salty Atlantic Waters that dominate the south show the deepest winter mixed layers (~500m) while the north and
21 northeast show shallower depths (~100m). Based on the decomposition of total stratification into temperature and salinity
22 contributions, we find that, the subsurface stratification is mainly controlled by temperature in the south, by salinity in the
23 northwest, while in the north, the North Icelandic Irminger Current and East Icelandic Current alternate seasonally, shifting
24 the region between temperature-dominated and salinity-dominated stratification. The interannual variability of the mixed
25 layer and of its thermohaline properties is also large around Iceland. Mixed layer waters were generally colder in the 90's,
26 then warmed until approximately 2015, and became colder again from 2015 to 2018. In the northeast, a multidecadal mixed
27 layer warming trend emerges from the interannual variability as the Atlantic Water progresses northeastward, which is
28 responsible for transforming locally the upper stratification from salinity-dominated into temperature-dominated. This is
29 associated with the “Atlantification” of the Arctic. Within the mixed layer south of Iceland, density has continuously
30 decreased since the mid 1990's. Elsewhere, we observe density-compensated changes in mixed layer temperature and
31 salinity, without clear long trends. This study provides an unprecedented and detailed description of the seasonal to multi-
32 decadal variability of the mixed layer depth and stratification around Iceland, showing links between this regional
33 variability and changing North Atlantic under global warming.

34 **Keywords:** Mixed layer depth, Mixed layer properties, stratification, Ocean warming, Atlantification, Interannual
35 variability

36

37 1 INTRODUCTION

38 The ocean around Iceland is a key region where major water masses and currents interact, shaping the North Atlantic
39 circulation and play a crucial role on the Atlantic Meridional Overturning Circulation (AMOC). The Nordic Seas are among
40 the few places on the globe where the formation of deep waters (1000-3000 m depth) occurs during winter deep convection
41 (Petit et al., 2020). The southern end of the Nordic Seas is bounded by the Greenland-Iceland-Scotland Ridge (GISR). The
42 North Atlantic Current (NAC) brings the warm and salty Atlantic Water (AW) northward into the Nordic Seas (Hátún and
43 Chafik, 2018; Østerhus et al., 2019; Hátún et al., 2021). The AW crosses the ridge in three ways (Fig. 1): (i) between
44 Greenland and Iceland, where the Irminger Current (IC) forms the North Icelandic Irminger Current (NIIC) bringing AW
45 that flows clockwise around Iceland (Jónsson & Briem, 2003; Jónsson & Valdimarsson, 2012); (ii) between Iceland and
46 the Faroe Islands (Mauritzen, 1996); and (iii) through the Faroe Shetland Channel (Hansen and Østerhus, 2000; Hansen et
47 al., 2023), contributing up to 48% of the total AW transport. The AW undergoes strong cooling and densification in the
48 Nordic Seas and the Arctic Ocean (Mauritzen, 1996; Pérez-Hernández et al., 2019; Athanase et al., 2020; Huang et al.,
49 2023). This modified AW is referred to as Atlantic-origin Overflow Water (AtOW; e.g., Havik et al., 2017; Casanova-
50 Masjoan et al., 2020) and is one of the two sources of Denmark Strait Overflow Water (DSOW; Semper et al. 2019). AtOW
51 travels southward as a mid-depth water mass in the East Greenland Current (EGC; Håvik et al., 2017), from where, part of
52 it diverts east and merges with the NIIC northeast of Iceland (Casanova-Masjoan et al., 2020).

53 The transformation of AW into AtOW takes place in different areas of the Nordic Seas: along the Norwegian Current
54 (Håvik et al., 2017), in the Iceland Sea Gyre (Våge et al., 2013), on the eastern side of Greenland, or even -due to its
55 proximity- in the Arctic Basin (Pérez-Hernández et al., 2019). This transformation has different driving mechanisms
56 impacting mixing and convective processes. Wind-stress, sea-ice retreat and high heat loss due to cold-air outbreaks drives
57 the transformation east of Greenland (Våge et al., 2018), sea-ice retreat and heat exchange dominate north of Svalbard
58 (Pérez-Hernández et al., 2019; Athanase et al., 2020), and heat fluxes are the main drivers in the center of Iceland Sea
59 (Våge et al., 2013). Thus, the Nordic Seas region has been previously described as a “mixing pot” (Renfrew et al., 2019),
60 largely responsible for the overall formation of deep overflow water (Lozier et al., 2019). The Nordic Seas are also a large
61 repository of freshwater, primarily originated from glacier melt and river discharge. This water mass increases buoyancy
62 and is carried southward by the East Greenland Current (EGC). Therefore, it is crucial to fully understand the variability
63 of the upper ocean, where mixed layers (ML) develop and transform these water masses.

64 The Arctic Ocean is warming much faster than the global average, a process known as “Arctic Amplification,” which is
65 also associated with the “Atlantification” of the Arctic (Polyakov et al., 2017; Dai et al., 2019). While the causes are still
66 debated, Arctic Amplification has evident consequences, such as a decrease in seasonal sea-ice extent and a weakening of
67 the cold halocline (Polyakov et al., 2020; Dai et al., 2019). Although these changes are less pronounced in the central
68 Iceland Sea, similar processes have been observed in the central Greenland Sea and the northeastern shelf (Gjelstrup et al.,
69 2022; Strehl et al., 2024), suggesting that Atlantification may also influence the Iceland Sea. Changes in temperature and
70 salinity in the upper ocean modify upper-ocean stratification, which partially controls the mixed layer depth (MLD).

71 The depth and structure of the ML is primarily controlled by local buoyancy forcing, i.e., surface heat loss and freshwater
72 fluxes, which modifies the water density (Kohler et al., 2018). For instance, within the Iceland Basin, wintertime buoyancy
73 loss drives deep convection, shaping the thermohaline properties that influence the lower limb of the AMOC and its
74 variability in the subpolar North Atlantic (Petit et al., 2021). The pre-existing stratification of the water column is
75 responsible for controlling the effect of the surface forcing. Strongly stratified upper layers resist mixing, while weak
76 stratification allows deeper penetration of turbulence and convection mixing (Pierce et al., 1986). Over shorter timescales,
77 on the order of days, the MLD can significantly deepen as a result of the strong wind events with significant wind stress

78 and associated large wave heights (Skylvingstad et al., 2023). MLD and stratification are strongly influenced by
79 atmospheric forcing, including variability associated with the North Atlantic Oscillation (NAO), which modulates wind
80 stress, surface heat flux, and freshwater input in the Iceland region (Hurrell, 1995; Dickson et al., 1996)

81 The IPCC report indicates with *high confidence* that roughly 40% of the global ocean mean upper ocean stratification
82 has increased about 3.3–6.1% since 1960 due to both oceans warming and high-latitude freshening (Tesdal et al., 2018;
83 Yamaguchi and Suga, 2019; Bindoff et al., 2019; Liu et al., 2020; Sallée et al., 2021). Increased stratification is associated
84 with less efficient diapycnal mixing, reducing the exchanges of heat and tracers from the mixed layer into the ocean interior.
85 It has also been observed, with *high confidence*, that the ML is undergoing changes (Bindoff et al., 2019; on Climate
86 Change, IPCC). Particularly, the shallow summertime ML, which is more likely to be affected by global warming, is
87 deepening at a rate of 5 – 10 m per decade (Sallée et al., 2021). Despite the reported global patterns, it has been also
88 acknowledged that regional changes might differ from the global estimates (Fox-Kemper et al., 2021).

89 The warming of the ML and the associated increase in stratification have an impact in biogeochemical processes like
90 phytoplankton blooms and carbon or oxygen sequestration, key components for the Earth’s climate (Olafsson, 2003; Pérez
91 et al., 2021). In the waters surrounding Iceland, the phytoplankton community is closely linked with the water mass
92 properties and hence, an “Atlantification” will replace Polar communities with more Atlantic communities (Cerfonteyn et
93 al. 2023). In the Arctic Ocean, north and northwest of Iceland, the early onset of stratification in spring gives rise to rapid
94 shallowing of the mixed layer and triggers early spring phytoplankton blooms, whereas the weakly stratified water-column
95 in the Atlantic water and the associated deep ML delay the spring bloom south of Iceland (Zhai et al., 2012). This also has
96 strong consequences in carbon uptake, vertical nutrient supply and biological processes (Yamaguchi and Suga, 2019).
97 Other indirect impacts of the increased stratification include changes in upwelling, deep-water formation rates, biological
98 production, and remineralization rates (Holt et al., 2016), and deoxygenation (Shepherd et al., 2017).

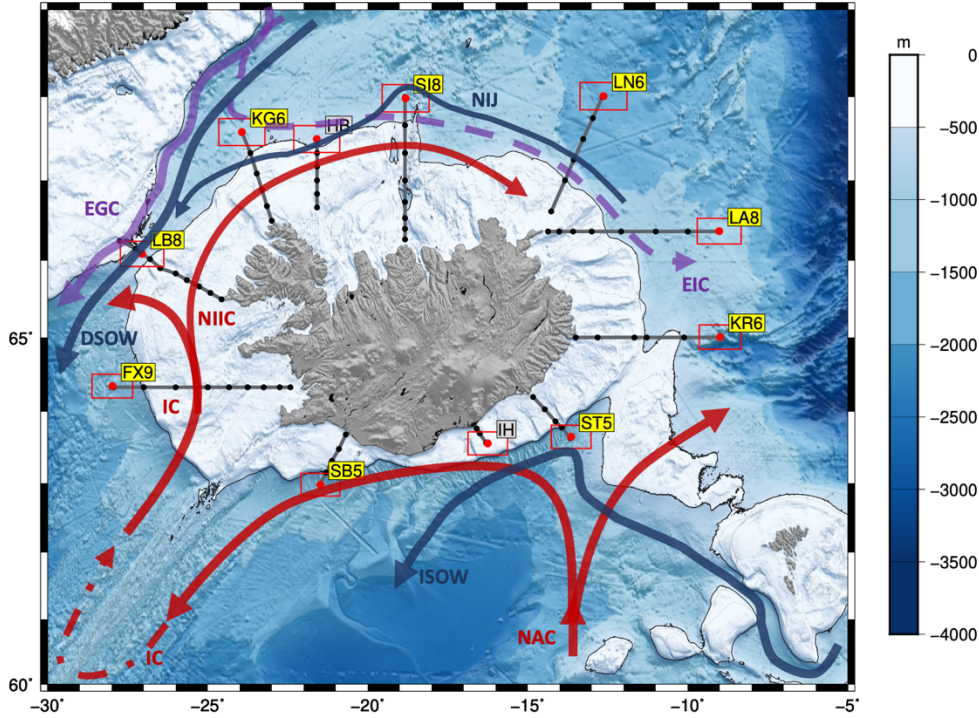
99 Thus, the overall goal of this study is to characterize the spatial and temporal variability of the mixed layer and
100 stratification around Iceland, where Atlantic Water inflow, Arctic waters, and local surface fluxes shape upper-ocean
101 properties. Using a 29-year hydrographic time series, we investigate the variability of water-mass properties, mixed-layer
102 depth (MLD), density, and thermohaline structure across seasonal and interannual timescales. We examine correlations
103 with atmospheric circulation patterns such as the North Atlantic Oscillation (NAO) and, to complement the observations,
104 use a 1D PWP model to simulate the mixed-layer response to local forcing, helping to identify the mechanisms driving
105 MLD variability.

106 2 DATA AND METHODS

107
108 We use Conductivity-Temperature-Depth (CTD) data from the repeated hydrographic observational program of the
109 Icelandic Marine and Freshwater Research Institute between 1990 and 2019. The oceanographic surveys took place
110 quarterly, mainly in February, May, August, and November with little coverage during the intermediate months.
111 Observations are made at standard repeated sections. The profiles are obtained with a Seabird 911plus CTD mounted on a
112 rosette with Niskine bottles. The conductivity data are calibrated with salinity samples taken at the bottom of each station.
113 All sensors underwent regular calibrations by the manufacturer.

114 In our analyses we considered only the deepest stations in each section (red dots in Fig. 1), including nearby stations
115 within an area defined by $1^\circ \times 0.5^\circ$ in longitude and latitude (red boxes). The selected stations are located outside of the
116 Icelandic shelf (about 500 m depth). This criterion was chosen to avoid topographic effects, such as across shelf processes

117 on the stratification of the water column and to avoid MLDs limited by shallow bathymetry. Thus, the stations in gray, HB
 118 and IH in Figure 1 were not considered as they fall on the shelf. For the sake of simplicity stations will be named with the
 119 acronym of the standard section, first two letters and the station number. The station full name (section and station number)
 120 can be found in Table 1.



121
 122 **Figure 1: Map of the typical hydrographic sections collected by the Marine and Freshwater Research Institute around Iceland; the**
 123 **black dots represent the nominal location of the standard stations from 1990-2019. The red dots are the stations used for this analysis**
 124 **and the red boxes delimit the area within which all data were considered for this study. The grey bathymetric contours are spaced**
 125 **every 100 m for the shallow water until the 500 m depth (thick black line) and then every 500 m. The hydrographic stations shown**
 126 **in the yellow boxes corresponding to the standard sections: Faxaflói (FX9), Látrabjarg (LB8), Kögur (KG6), Hornbanki (HB),**
 127 **Siglunes (SI8), Langanes NE (LN6), Langanes E (LA8), Krossanes (KR6), Stokksnes (ST5), Ingólfshöfði (IH) and Selvogsbanki**
 128 **(SB5). The gray labeled IH and HB were not used in this analysis. The main surface and deep currents are also depicted on the map.**

129 In this study we analyze the inter-annual variability and linear trends of the ML over a 29-year period as well as the
 130 seasonal variability using the seasonal extremes (summer and winter), when there is more data coverage. From the CTD
 131 stations we estimated the MLD using the density threshold method with a criterion of $\sigma_\theta = 0.01 \text{ kg m}^{-3}$ (as, for instance,
 132 in Piron et al., (2016) in the Irminger Sea) and a reference depth of 10 m. We chose this criterion instead of the usual 0.03
 133 kg m^{-3} (de Boyer Montégut, 2004) as the latter overestimated the MLD in more than 500 visually inspected profiles (not
 134 shown). For comparison and robustness of our chosen method, we also estimated the MLD using other criteria (de Boyer
 135 Montégut et al., 2004; Holte et al., 2017). We found the density threshold method appropriate for our region as it proves to
 136 be effective even for cases where the variations of salinity and temperature were large. Those variations usually compensate
 137 in density making this method more suitable. We have validated our method against previous work by Våge et al., 2018,
 138 where a glider data was available, and the results were satisfactory. However, automatic detection methods have
 139 limitations, as they may miss, for example, stacked mixed layers and other non-canonical representation MLs.

140 For each profile we computed the Brunt -Väisälä frequency (N^2), defined as:

141
$$N^2 = g \frac{1}{\rho_0} \frac{\partial \sigma_\theta}{\partial z}, \tag{1}$$

142 where g is the acceleration due to gravity, ρ_0 is a reference density, σ_θ is the potential density and z is depth. N^2 can

143 be decomposed to show the relative contribution of salinity and temperature to the observed stratification as follows:

144

$$145 \quad N^2 = N_T^2 + N_S^2, \quad (2)$$

146 where N_T^2 and N_S^2 are the components representing the stratification set by the temperature and salinity, respectively and
147 are defined as:

$$148 \quad N_T^2 = g \left(\alpha \frac{\partial T}{\partial z} \right), \quad (3)$$

149

$$150 \quad N_S^2 = g \left(\beta \frac{\partial S}{\partial z} \right), \quad (4)$$

151 where α is the thermal expansion coefficient and β is the haline contraction coefficient at constant pressure. This
152 decomposition has also been made to classify the oceans by their stratification contribution into α -ocean, β -ocean, and
153 transition zone, where in α -oceans stratification is permanently dominated by temperature, in β -oceans by salinity and the
154 transition regions are either intermittently or seasonally dominated by temperature or salinity (Carmack, 2007; Stewart and
155 Haine, 2016). For the water column to be statically stable, N^2 must be positive. However, the contributions may not be
156 positive; when any of its components, N_T^2 or N_S^2 are negative, temperature or salinity respectively has a destabilizing effect
157 on the resulting stratification that must be compensated by the other variable to maintain a stable water column. Small
158 values of N^2 indicate that the water column is weakly stratified which favors mixing due to winter convection and deeper
159 MLD.

160 To investigate further the driving mechanism of the MLD we used the Price-Weller-Pinkel (PWP) one-dimensional
161 model (Price et al., 1986). The PWP model is a one-dimensional vertical model used to simulate the evolution of the ocean
162 mixed layer in response to atmospheric forcing, including wind stress, heat fluxes, and freshwater fluxes. The model
163 evolves vertical profiles of temperature, salinity, density, and horizontal velocity based on surface forcing and a set of
164 physical stability criteria. The first criterion is convective overturning. If surface cooling increases the density such that
165 the water column becomes gravitationally unstable (i.e., denser water overlies lighter water), the model applies vertical
166 mixing until static stability is restored. The second criterion is based on the bulk Richardson number, which represents
167 wind-driven mixing. The mixed layer deepens until the bulk Richardson number ($R_{ib} = (g\Delta\rho h) / (\rho_0(\Delta U)^2)$) reaches or exceeds
168 the critical values 0.6. The final criterion is the Gradient Richardson Number $R_{ig} = N^2 / (\partial U / \partial z)^2$ which accounts for shear
169 instability. When $R_{ig} < 0.25$ local vertical mixing is applied. The PWP model is initialized with ERA-5 12-hour dataset of
170 wind stress, heat, and freshwater fluxes (Hersbach et al., 2020) and the summer/winter averaged vertical profiles of
171 temperature and salinity from the observations presented here (Fig. S1-S3). The 1D model allows to address the relative
172 contributions from diurnal heating/cooling, freshwater fluxes, and wind mixing.

173

174 In addition, we broaden the impact of our findings by using the hydrographic database published in Brakstad (2023)
175 that includes, in addition to the dataset from the Marine and Freshwater Research Institute of Iceland, other multiplatform
176 observations like Argo floats or cruise data between 1950 and 2019. For this objective, a larger oceanic region is used and
177 classified into α -ocean and β -ocean using the spice frequency, K^2 , (Carmack, 2007; Strehl et al., 2024), defined as:

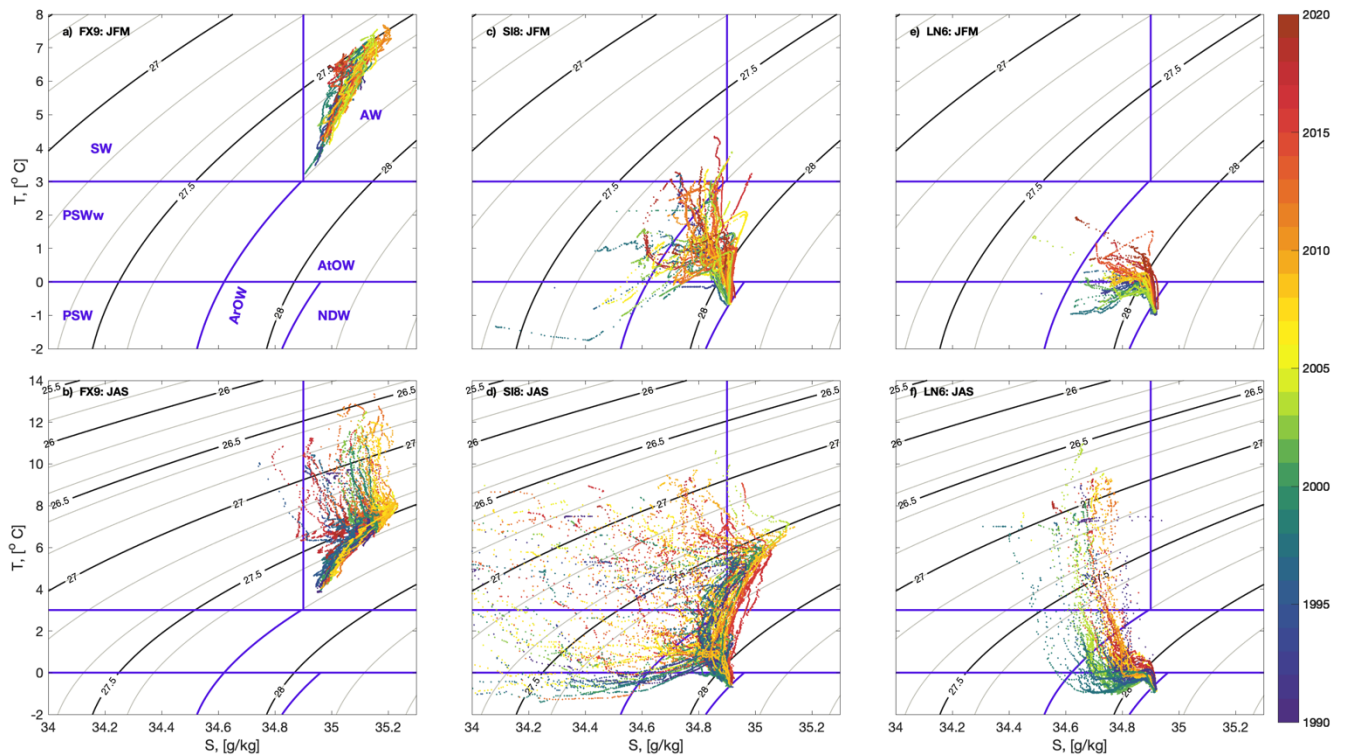
$$178 \quad K^2 = N_T^2 - N_S^2. \quad (5)$$

179 K^2 is positive (negative) in α -(β -)oceans.

182 3.1 Hydrographic properties around Iceland

183 The hydrographic properties (potential temperature-salinity diagrams) around Iceland show important spatial, seasonal
 184 and interannual variability are shown in Figure 2; the T/S properties differ widely between the three representative stations:
 185 FX9, SI8 and LN6 for the west, north and northeast of Iceland. FX9, in the southwest of Iceland, is completely dominated
 186 by Atlantic Water (AW; Fig. 2 a and b). At SI8, in the north, the dominating water masses in winter are of polar origin, i.e.,
 187 warm Polar Surface Water (PSWw) in the upper layers, and Atlantic Overflow Water (AtOW) and Arctic Overflow Water
 188 (ArOW) in the intermediate/bottom waters (Fig. 2c and d). The SI8 station also presents the largest variance of its
 189 thermohaline characteristics. It is noteworthy that using fixed definitions of water masses may lead to biased estimates, as
 190 these water masses have been steadily warming over the past two decades. LN6, in the northeast, contains the coldest and
 191 densest waters on average (Fig. 2c and f).

192



193

194 **Figure 2: (Top row) Winter (JFM) and (bottom row) summer (JAS) T-S diagrams for three selected stations (a, b) FX9, (c, d) SI8**
 195 **and (e, f) LN6, considered as representative for the south, north and northeast regions shown in Fig. 1. The T-S individual profiles**
 196 **are color-coded by year. The main water masses as defined in Table 2, are labeled in panel (a).**

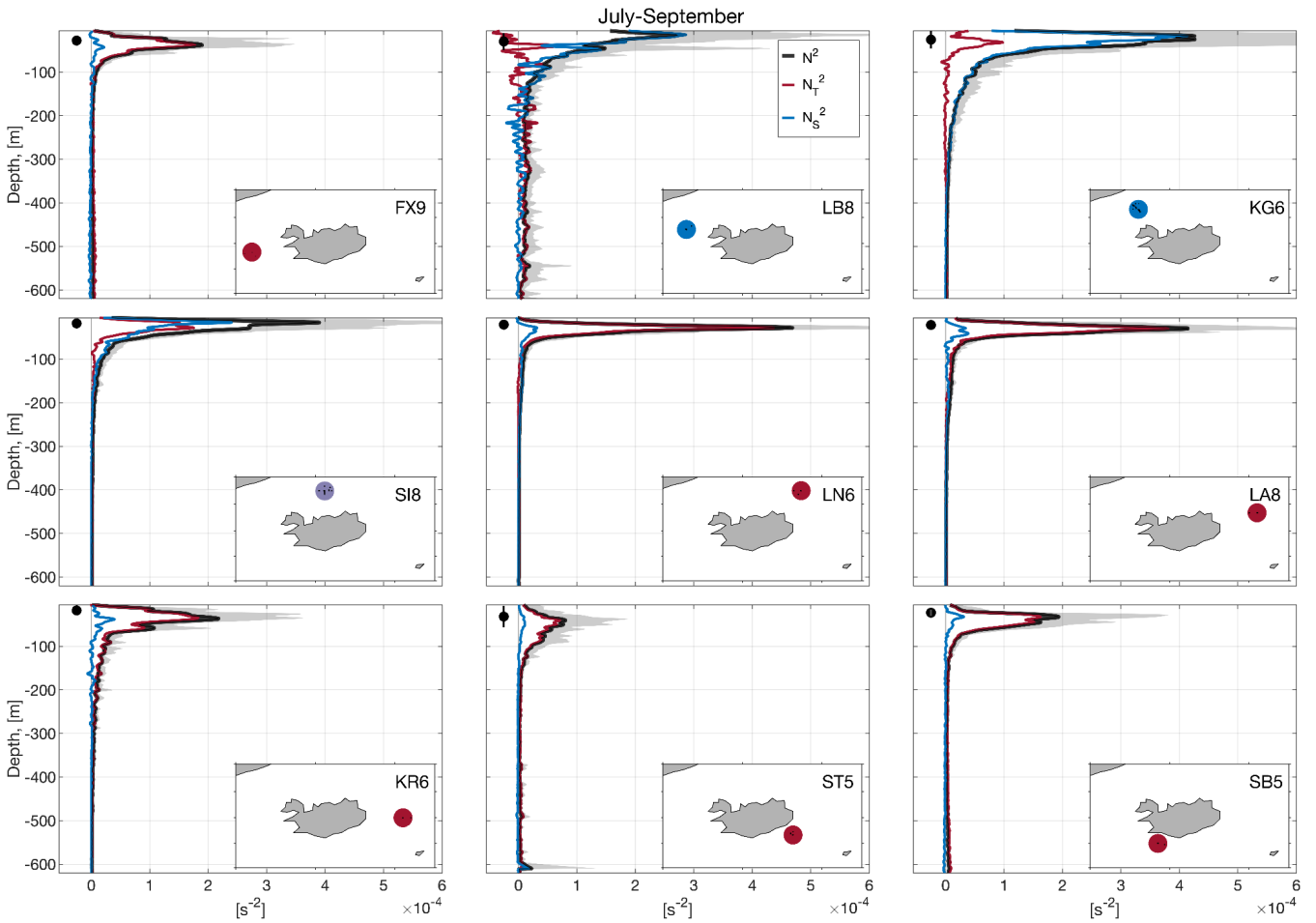
197 The three stations have a clear seasonality. Overall, due to seasonal warming of the upper layers, the summer profiles
 198 span a wider temperature range (Fig. 2b, d, f) than in winter (Fig. 2a, c, e). FX9 is notably warmer and saltier than the other
 199 stations, especially in summer (Fig. 2a), when the minimum temperature in FX9 (nearly 4°C) is as high as the maximum
 200 temperature in SI8 and 2 degrees higher than in LN6 (Fig. 2a, b, c). At SI8 a large change in density between seasons is
 201 observed mainly driven by the contribution of AW, explained by offshore migration of the NIIC and the stronger inflow of
 202 AW during the summer (Fig. 2c, and f) (Jónsson and Valdimarsson, 2012). While the widest seasonal amplitude in salinity
 203 is observed at SI8, the largest seasonal amplitude in temperature is observed at LN6.

204 FX9 does not show a clear interannual pattern in summer but in winter the 2000's are strikingly saltier than the other
205 years. In contrast, at SI8 and LN6 fresher and colder waters are observed in the 90's, they progressively warm and become
206 saltier over time, and they reach their maximum temperature and salinity by 2015-2018. This decadal pattern is more
207 evident in winter, but it is observed in both seasons.

208 3.2 Seasonality of Stratification and Mixed Layer Depth (MLD)

209 The spatial and temporal variability of the stratification around Iceland is remarkably large (Fig. 3 and Fig. 4), and the
210 relative contribution of temperature and salinity shows a strong seasonal cycle. In summer, the MLD is relatively shallow,
211 oscillating around 50 m with a small standard deviation (Fig. 3). In contrast, in winter the ML reaches depths greater than
212 400 m in FX9, ST5 and SB5 with large standard deviations spanning a 100 m range (Fig. 4). The deepest average MLD is
213 found in FX9 while the shallowest are KG6, SI8, LA8 and KR6.

214 In summer (Fig. 3), the upper-ocean stratification around Iceland (Fig. 3) is generally dominated by temperature, except
215 for the three northwestern stations (namely LB8, KG6, SI8). LB8 exhibit the largest variability in both N_T^2 and N_S^2 , but is
216 mainly dominated by salinity in the upper 200 m and by temperature below that depth. This transition station is located at
217 the sill of Denmark Strait, a convergence zone for several currents (see Table 1 and Fig. 1) carrying water masses with
218 contrasting T-S properties within the ML and the thermocline (Jónsson, 1999; Logemann et al., 2013; Casanova-Masjoan
219 et al., 2020). In KG6, the fresh inflow from the EGC compensates for the cold temperature, and salinity largely dominates
220 stratification. For SI8, we observe a mixed regime with almost equal contributions from both salinity and temperature to
221 the total stratification, which suggests that this is also an area of transitional regime. For the stations: LN6, LA8 and KR6,
222 despite the fact that stratification is mainly dominated by temperature, exhibit a small subsurface contribution of salinity
223 just below the ML, likely due to the presence of fresh PSWw. The southern stations ST5 and SB5, have a minimal
224 contribution to stratification from salinity, which may be associated with the numerous river discharges and the proximity
225 to the continental shelf. The river discharge is the largest near SB5, likely explaining the summer subsurface contribution
226 to salinity (Whitney, 2025).



227

228

229

230

231

232

233

Figure 3: Summer (JAS) average density stratification (N^2) profiles for the selected stations; the average total stratification (black) is decomposed into temperature (red) and salinity (blue) contributions, while the gray shaded band represents all the stratification profiles. The black solid dot (left of the profiles) represents the average MLD with the error bar showing the standard deviation as an indicator of the temporal variability. The maps in the lower corner show the location of the station within a circle color coded by the dominating regime according to the contribution to stratification: red for temperature, blue for salinity, and purple for a mixed regime.

234

235

236

237

238

239

240

The hydrographic conditions are very different for winter; the stratification is one order of magnitude lower, i.e., comparing Figure 3 and Figure 4. Also, the water temperature is much colder due to winter heat loss. Under these conditions, the relative contribution of salinity to the total stratification stands out around Iceland except at the southern stations (FX9, SB5, ST5), where the weakest winter stratification is observed. This southern region shows the deepest MLD, between 350 and 700 m in the stations FX9, SB5 and ST5, while for the northern stations (KG6, SI8, LN6, LA8, and KR6) the mean winter MLD is about 100 m. Similar to summer, station LB8, also shows high variability in winter stratification, associated with the confluence of currents at the Denmark Strait.

241

242

243

244

245

246

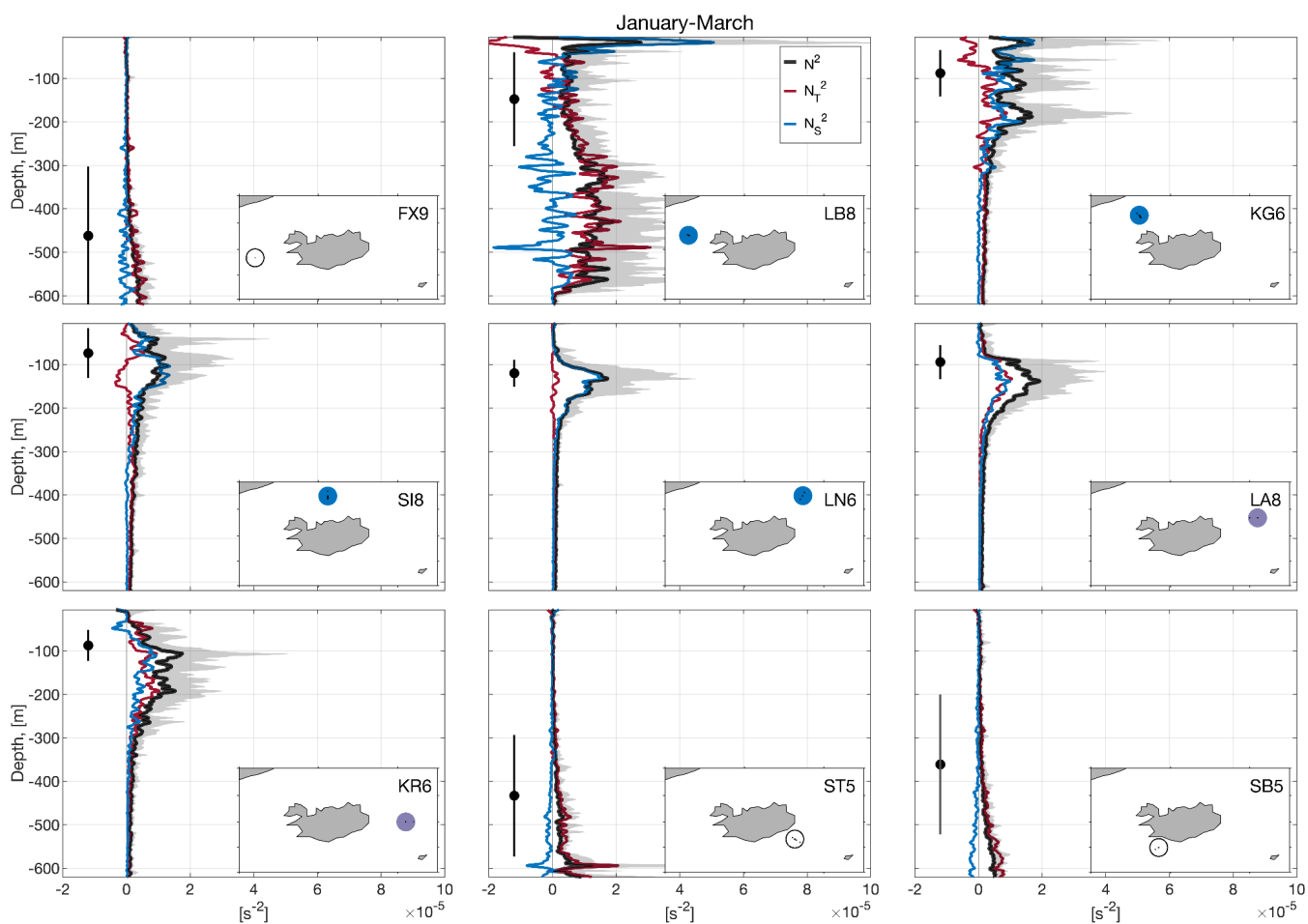
247

248

249

The role of temperature or salinity in setting the stratification (α - and β - ocean, see *e.g.*, Carmack, 2007) is linked to the hydrographic characteristics (temperature and salinity) of the dominant water masses within each region. Based on this, we can classify the waters around Iceland. The southern side is an α -ocean as it receives the influence of warm and relatively salty AW. Hence, the stratification is mainly temperature driven in both seasons (see FX9, ST5 and SB5 in Figures 3 and 4) and MLD gets deeper than 400 m in winter. The northwest of Iceland (LB8, KG6) is under the influence of the EGC throughout the year bringing fresh PSW and PSWw into the area. Therefore, this area with winter MLDs of 100-150 m can be considered a β -ocean, with heat fluxes equivalent to the southern region but with stronger and salinity dominated stratification blocking the potential for deep convection, i.e., this region does not have a mechanism to lose surface buoyancy seasonally in the salinity component. In contrast, the northeastern Icelandic area (SI8, LN6, LA8 and KR6) shifts

250 from β in winter to a mixed α/β in summer. This is likely due to an offshore migration of the NIIC increasing the inflow of
 251 AW (Jónsson and Valdimarsson, 2012; Casanova-Masjoan et al., 2020, their Figure 11). For instance, in winter, SI8 has a
 252 PSW signature at the thermocline with salinity driving the stratification and a MLD of about 90 m (β -ocean), and in summer,
 253 the NIIC brings warm AW to the upper layers of SI8 making the stratification similarly driven by temperature and salinity.
 254 Overall, the north of Iceland exhibits the strongest summer stratification of the study area which results in very shallow
 255 MLDs.



256
 257 **Figure 4: Same as Figure 3 but for winter (JFM). The white color circles shown in the maps of stations ST5, SB5, and FX9 indicate**
 258 **very weak winter stratification with no significant contribution of salinity or temperature.**

259 3.3 Interannual to decadal variability of the mixed layer properties

260 To investigate the interannual to decadal ML variability we focused on three reference stations, considered representative
 261 of the α -ocean (FX9, West), transition (SI8, north) and β -ocean (LB8, northwest) regimes around Iceland. FX9 dominated
 262 by relatively warm and salty AW, SI8 as a transition area, and LB8 dominated by cold and fresh PSW. The three stations
 263 show strong interannual variability.

264 In FX9, to the West of Iceland, there is a correlation ($R=0.69$ p -value <0.01) between mixed layer temperature (MLT)
 265 and salinity (MLS) anomalies. Between 1990 and 1998 the mixed layer was the deepest, the coldest, and the second freshest
 266 period, as shown in Figure 5a, and d (positive MLD anomalies correspond to deeper ML and negative ones correspond to
 267 shallower ML). Around the period 2000-2014, there is an increase in MLT and MLS as the ML becomes moderately
 268 shallower. The winter MLD is the shallowest, saltiest, and warmest in 2010 (Fig. 5a, and d), where the temperature
 269 contribution seems to control this minimum. From 2015 to 2018 the ML returns to the cold and fresh conditions of the 90's
 270 but the MLD is average. The observed variability of the ML and its temperature in FX9 exhibits correlation (R) with the
 271 North Atlantic Oscillation (NAO); for MLD, the best correlation was $R=0.53$, p -value <0.01 at lag zero; for MLS $R=-0.52$,

272 p-value<0.01 at lag -2 years (NAO leading), and for MLT $R=-0.49$, p-value<0.01 at lag -1 year (NAO leading (Fig. 5g, h).
 273 However, we consider that a 2-year lag lacks a realistic physical explanation; thus, we prefer to not to consider this as a
 274 reliable correlation. More qualitatively, positive NAO at the beginning and the end of the time series, corresponds with
 275 deeper colder and fresher MLs, while negative NAO between 2000 and 2015 roughly corresponds with shallower, warmer,
 276 and saltier MLs. As shown in Figure 2, FX9 contains only AW (Fig. 2a, d) likely advected from the south to the area by
 277 the Gulf Stream and later the Irminger Current. Similar conditions have been observed in the Irminger Sea over the same
 278 period, and they have been related to the NAO phase and its impact on the Subpolar gyre (Feucher et al., 2022). This
 279 suggests that the FX region is largely influenced by the Atlantic climate and therefore it is partly impacted by the NAO
 280 (Bersch, 2002).

281 At SI8, in the north of Iceland (Fig. 5b, e, h), the negative winter MLD anomalies are on the order of those at FX9 and
 282 also exhibit strong interannual variability without an identifiable pattern. Strong positive MLD anomalies are observed in
 283 particular years (e.g., 2000, 2007, and 2016) but they do not seem correlated with the MLT/MLS or with the NAO
 284 variability. Interestingly, the MLT and MLS co-vary during the period 1990-2005, when the mixed layer is colder and
 285 fresher, but this correlation weakens from 2005 to 2018, when the positive MLT anomalies increase while the MLS
 286 anomalies, although positive, do not vary significantly.

287 In LB8 (northwest), the winter MLD has the largest variability as the station is located in the vicinity of the front between
 288 NIIC and the EGC, which shapes the Polar and Atlantic conditions. Despite this large variability, a co-variance between
 289 MLT and MLS anomalies seems to be correlated with the position of the front. Fresher and colder MLs are associated with
 290 EGC influence and warmer/saltier MLs with the presence of NIIC (Fig. 5c, f, i). Generally, shallower MLs are also fresher
 291 and colder, which agrees with a salinity-dominated stratification in the upper layer (Fig. 4b). Three particular years present
 292 relatively deep, cold, and salty MLs: 1996, 2006 and 2014. The observed interannual variability in the ML and its properties,
 293 while large, does not seem to be correlated with the NAO, except the last decade where the high state of the NAO is
 294 consistent with the positive MLT and MLS, suggesting a larger presence of the NIIC at this station.

295



296
 297

298 **Figure 5: Interannual winter (JFM) variability from 1990 to 2019 in three stations representative of different regions around**
 299 **Iceland: (a, b, c) MLD anomaly (in percentage of its mean winter value over the whole record, green shading) and mixed layer**
 300 **temperature (MLT, blue bars). (d, e, f) Mixed layer salinity (MLS, grey bars) and winter average NAO index for comparison (purple**
 301 **shading). (g,h,i) Mixed layer density anomaly (MLrho, red bars) and Mixed layer density (kg/m^3), black dots. The represented**
 302 **stations are (a, d) FX9, in the southwest, (b, e) SI8, in the north, and (c, f) LB8 in the northwest. Positive anomalies in MLD, MLS,**
 303 **MLT, and MLrho correspond to deeper, saltier, warmer, and denser waters, respectively. The summary of the correlations is**
 304 **presented in Table 1.**

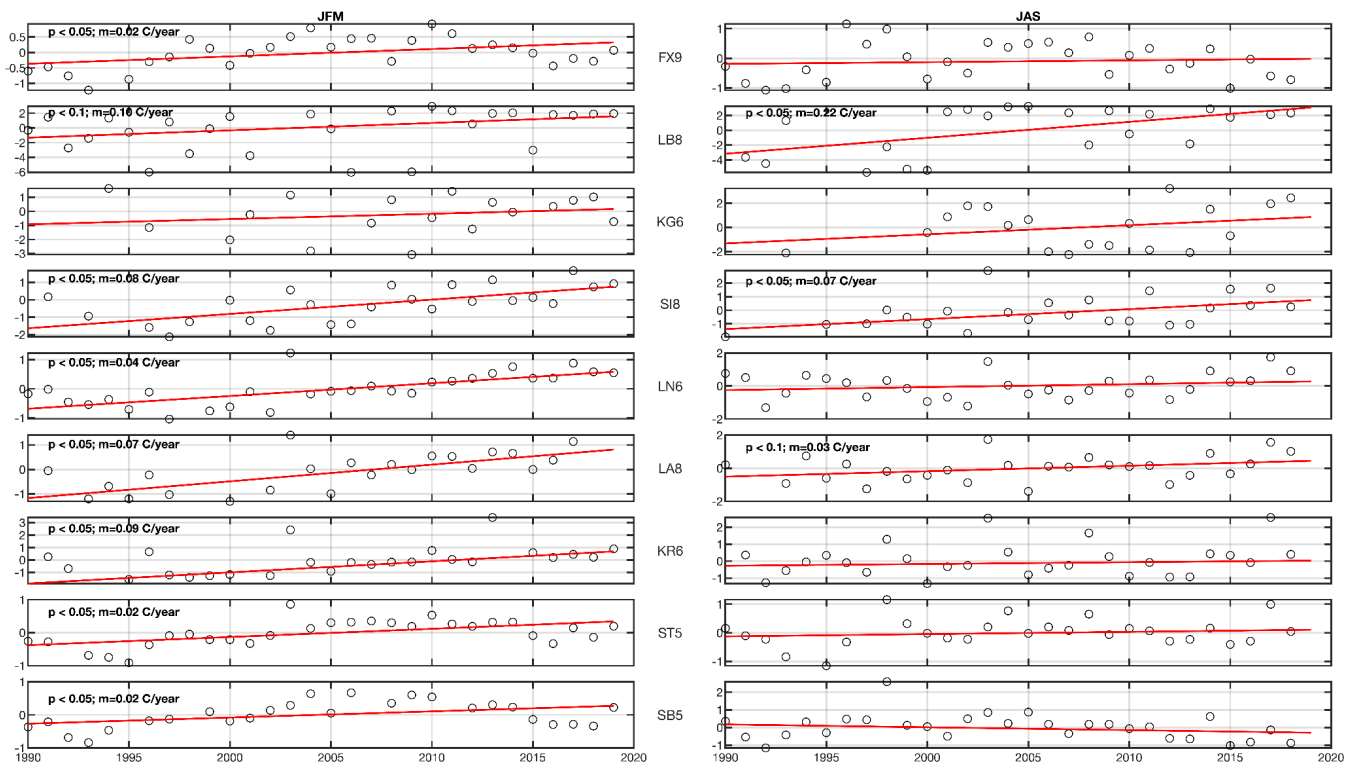
305 *Table 1. Pearson correlations between the different variables shown in Figure 5. Non-significant correlations are omitted. Displayed*
 306 *correlations are significant at 95% confidence ($p < 0.05$), and those significant at 99% ($p < 0.01$) are shown in bold.*

	FX9		SI8		LB8	
	Correlation	p-value	Correlation	p-value	Correlation	p-value
MLT-MLS	R=0.69	p<0.01	R=0.74	p<0.01	R=0.95	p<0.01
MLT-MLD	--	--	--	--	R=0.76	p<0.01
MLS-MLD	--	--	--	--	R=0.68	p<0.01
NAO-MLD	R=0.53	p<0.01	--	--	--	--
NAO-MLT	R=-0.41	p<0.003	--	--	--	--
NAO-MLS	--	--	--	--	--	--

307

308 To delve into the interannual to decadal variability of the MLT around Iceland, we analyzed its anomalies (relative to the
 309 long record) in all nine stations and computed their linear trends (Fig. 6). The temperature anomalies show significant
 310 interannual variability and spatial differences around Iceland. For instance, positive anomalies were observed in 2003 in
 311 most of the stations in both seasons, with particularly large temperature anomalies east of Iceland. Strong warm anomalies
 312 are also observed in 2017, mostly in summer at all stations except FX9 and SB5, located south of Iceland (Fig. 6; left panel).
 313 Although the 29-year period might be too short for identifying linear anthropogenically-driven trends, linear trends are
 314 significant in some of the stations, (where the p-value is indicated). The linear trends show a general warming of the mixed
 315 layer that is more evident in winter, mainly in the stations of the northeast (LN6, LA8). In the south (ST5, SB5 and FX9),
 316 even if the trend is significant from 2000-2015, there is an interannual variability that induces colder mixed layer conditions
 317 from 2015 to 2018. This tendency of returning to the conditions observed in the early 90's may be associated with the NAO
 318 (Feucher et al., 2022) as shown in Fig. 5. The observed general warming of the ML around Iceland is consistent with the
 319 progressive warming of the NIIC (Casanova-Masjoan et al. 2020).

320

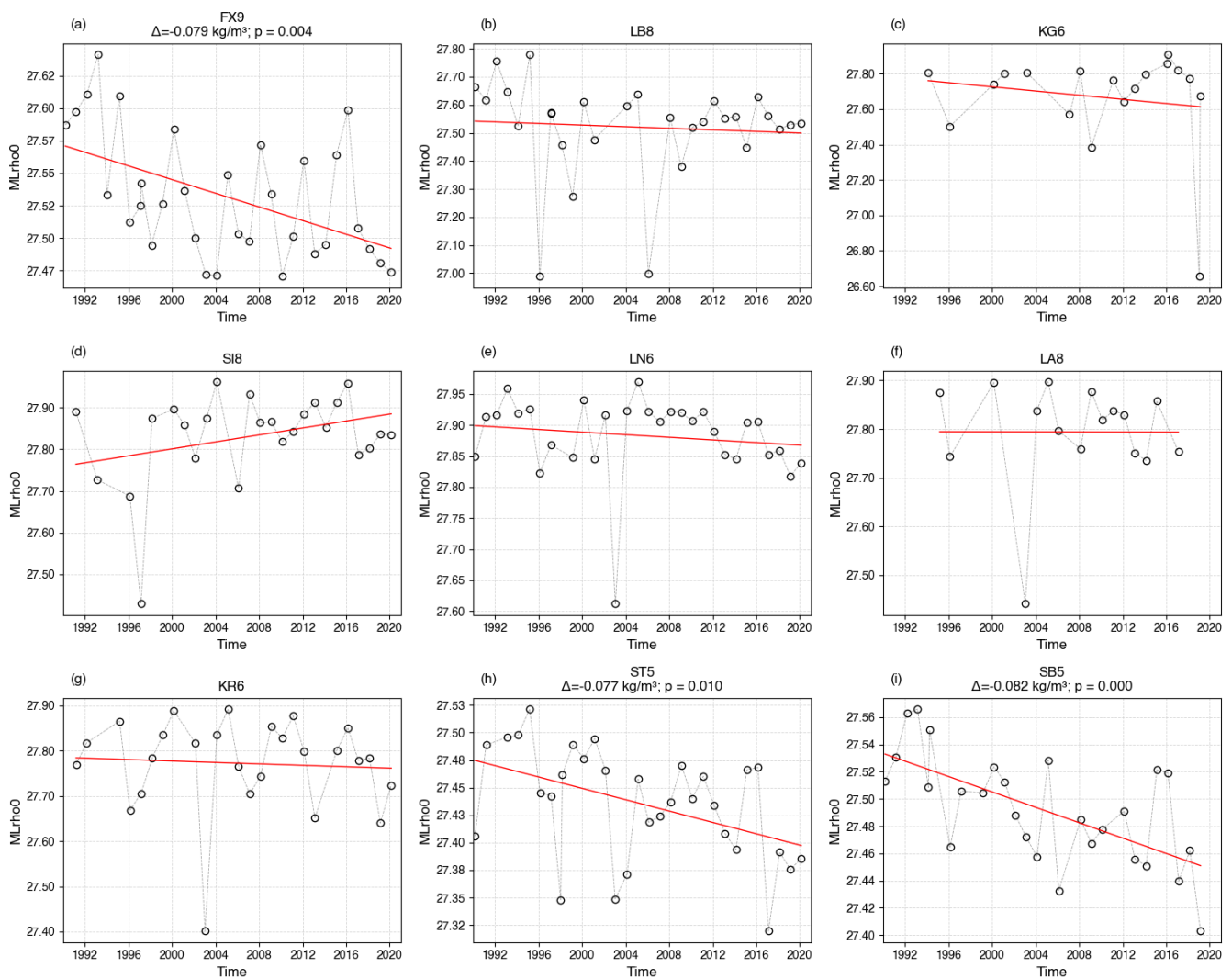


321
322
323
324

Figure 6: Mixed Layer Temperature (MLT) anomaly time series (left) winter (JFM) and (right) summer (JAS) for the 9 stations shown in Figures 3, 4. The anomalies show the p-values and the linear trends.

325
326
327
328

Similarly to Figure 6, in Figure 7 we compute the winter (JFM) density within the ML, which exhibits a statistically significant decrease for the stations in the south of Iceland (FX9, SB5, and ST5). The rest of the stations around Iceland do not show any significant changes. Remarkably, LN6, LA8, and SI8 show no change in density even though they experience a significant increase in temperature.



329

330

331

332

Figure 7: Mixed layer density (Mlrho) time series for the 9 representative stations only for winter (JFM). Stations FX9, ST5, and SB5 exhibit a statistically significant negative trend, with a total accumulated value of $\Delta \sim -0.08 \text{ kg/m}^3$ over the 30 years of observations.

333

4. MLD driving mechanisms from a 1D model

334

335

336

337

338

339

340

341

342

The summer stratification around Iceland in summer is roughly an order of magnitude higher than in winter, largely due to positive buoyancy forcing, resulting in shallower and more variable MLDs. Therefore, we study the atmospheric effect on these α - and β -ocean regions by implementing the Price et al. (1986) one-dimensional model. The model is forced starting in the fall before the deep MLD develops. It is worth mentioning that the 1D model estimates the MLD from temperature-based profiles while the estimates from observations are density threshold based. The model results of the MLDs shown in Figure 8 are within the range of the observed average \pm standard deviations (thick black dots and lines in Fig. 8). For most stations a spring shoaling of the MLD is driven by reduced heat fluxes, while the MLD remains relatively deep due to the wind-stress. The choice of PWP model was made to support the idea that β - and transition oceans do not develop deep mixed layers, which is shown in Figure 8.

343

344

345

346

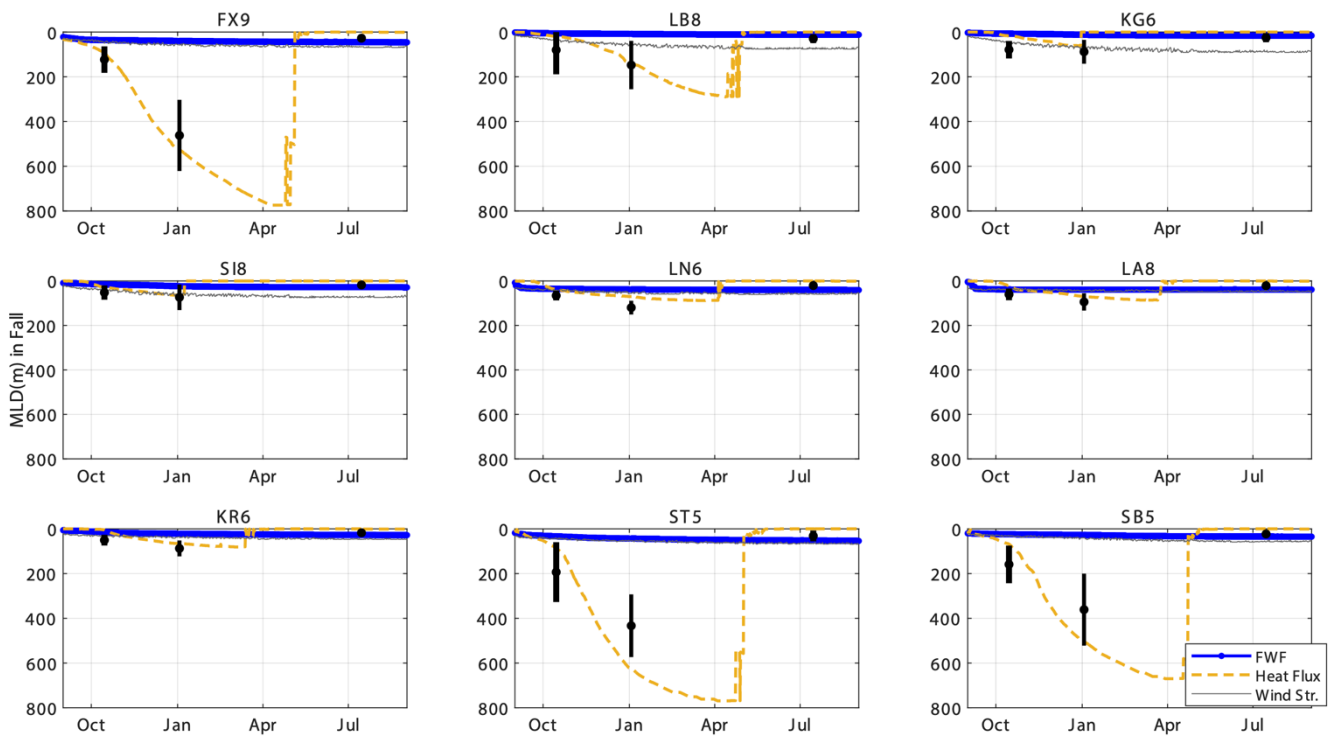
In the model, the stations embedded within the α -ocean with AW (Fig. 8: FX9, SB5 and ST5) present the largest MLDs exceeding 300 m depth, which is consistent with the observations. In this α -ocean region, the development of a deep ML is driven mainly by heat. However, within these stations, the wind-stress steadily contributes to the development of the ML. During the summer, shoaling of the mixed layer is likely influenced by the changes of both heat and freshwater fluxes, with

347 their effects on the MLD partially offset by wind stress (Fig. 8: FX9, SB5 and ST5).

348 The station LB8, despite being in Denmark Strait and presenting a large contribution of PSWw and PSW in the upper
349 layers (driving a β -ocean stratification), shows that the development of MLDs can be influenced by both, heat flux and/or
350 wind stress (Fig. 8: LB8). However, the contribution of wind-stress and freshwater cannot lead to MLDs deeper than
351 100m (Fig. S4:LB8). Beneath the PSW and PSWw at LB8 we find AtOW. Hence as the wind-stress develops, the MLD
352 evolution erodes the PSWw strata reaching the AtOW layer, allowing reduced heat fluxes to contribute to the MLD
353 development. This erosion is not visible on the stations embedded within the EIC.

354 Wind stress becomes the leading forcing mechanism northeast of LB8 at stations KG6, and SI8, coinciding with the shift
355 from α - to β - ocean stratification (Fig. 8). This region has a lower convective potential than regions with pure AW and
356 therefore does not produce large MLDs (Fig. 4 and 8). The MLD there results from roughly equal contributions of
357 convection and wind-driven mixing. At these stations, the best performance of the PWP model is obtained when both heat
358 flux and wind-stress are included (Fig. S4). Notably, the summer MLD remains shallow and roughly with the same order
359 of magnitude across all stations around Iceland (Fig. 8 and S4).

360



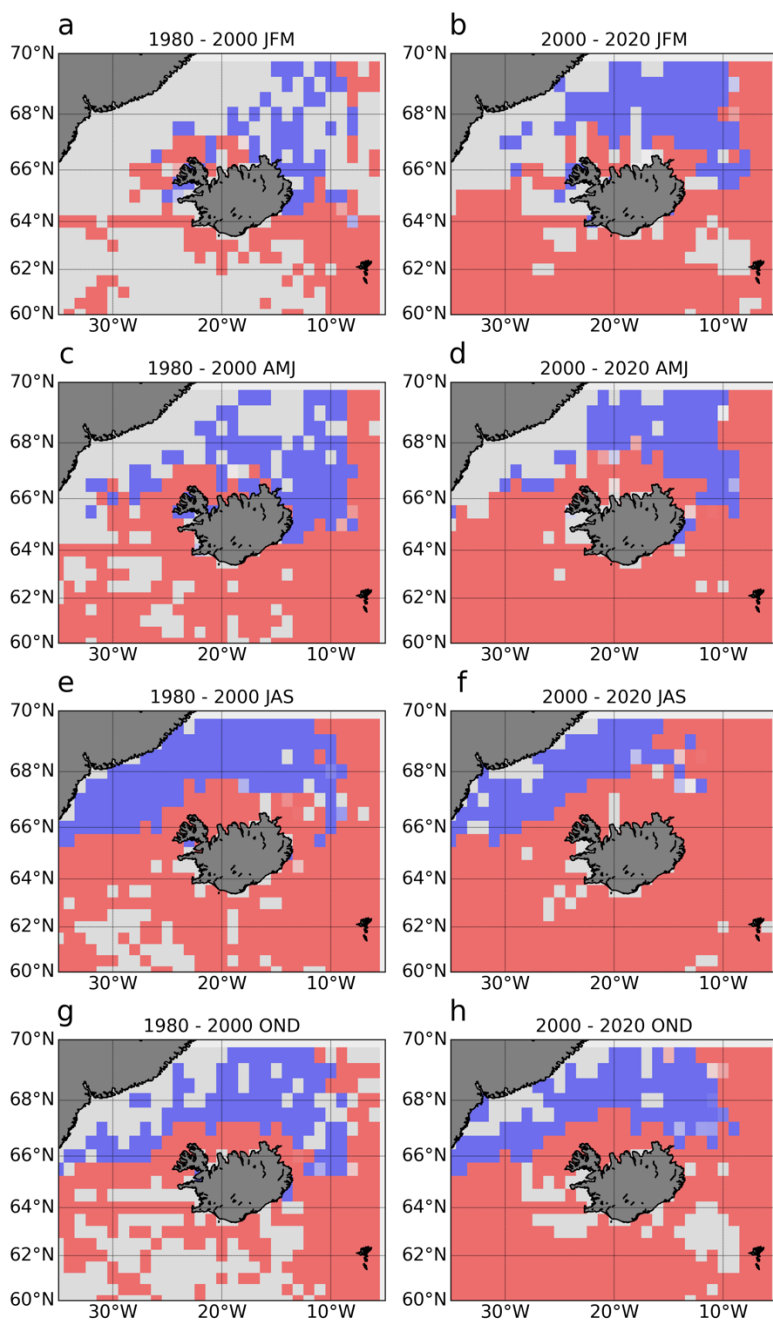
361

362 **Figure 8: MLD driving mechanism decomposition estimated from the PWP 1-D model (Price et al. 1986) for each of the studied**
363 **stations. Different MLD evolutions are shown for outputs forced with freshwater fluxes (blue), heat fluxes (red), and wind-stress**
364 **(green). Black dots represent the averaged winter and summer MLD with their standard deviations.**

365 5. Stratification around Iceland

366 To complement the understanding of the stratification of the Arctic and Subarctic waters around Iceland, their connection
367 with water masses, currents, and their variability, we used the spiciness frequency averaged in the first 200 m, estimated
368 following the methods described in Strehl et al. (2024) implementing Equation (5). For this analysis we used the
369 hydrographic dataset in Brakstad et al (2023). The spiciness distributions shown in Figure 9 reveal that temperature
370 dominates on the southern side of Iceland, marked by an α -ocean regime, while salinity dominates the northern side,

371 associated with β -ocean. These areas largely correspond with the distribution of AW versus PSW/PSWw (See Fig. 2 for
372 T-S definitions).



373
374 **Figure 9: Mean upper 200m spice frequency for the region of study showing the α -ocean (red) and β -ocean (blue) regions for the**
375 **periods of 1980-2000 and 2000-2020 and the four main seasons JFM (a,b), AMJ (c,d), JAS (e,f) and OND (g,h). The Brakstad et al**
376 **(2023) hydrographic dataset is used for this calculation.**

377 The seasonal distribution of spice frequency north of Iceland agrees with the seasonal behavior of the NIIC described in
378 Casanova-Masjoan et al. (2020) where the NIIC surface extension in winter and spring remains constrained to the northwestern
379 side of Iceland due to the cold southeast surface imprint of the EIC. Then in summer, the NIIC expands northeastward, reaching
380 all the way to the eastern side of Iceland and the northernmost station at the SI transect and constraining the polar water
381 between the northern end of the Kolbeinsey Ridge and the Greenland shelf. Then in fall the NIIC northern extension narrows
382 but is still able to surround Iceland. It is noteworthy that a clear increase in coverage of the α -ocean, mainly in summer, is
383 observed by comparing the 1980-200 average and the 2000-2010 average.

385 In this study, we discussed the seasonal and interannual variability of the mixed layer characteristics and the stratification
386 regimes around Iceland by using a long time series of CTD data. Based on our results, we propose the regionalization of
387 the waters around Iceland into three dynamical regions α -ocean, β -ocean, and transition-ocean.

388 The southwestern region is dominated by AW both in winter and summer. Within this region, the winter MLD
389 is the deepest and most variable of the whole study area, with ML's occupied by AW over the whole sampling period.
390 This region is influenced by the dynamics of the Irminger Sea and the Subpolar gyre and has favorable conditions (α -
391 ocean) for winter deep convection driven by heat fluxes to develop deep mixed layers, which agrees with previous
392 studies (Carmack, 2007; Våge et al., 2008; Piron et al., 2016; Stewart and Haine, 2016; Petit et al., 2020). In the
393 southern region, the ML salinity anomaly was negative over the last 5 years, which is consistent with previous
394 numerical models and Argo observations showing a freshening trend of the North Atlantic (Tesdal et al., 2018;
395 Holliday et al., 2020, Liu et al., 2020). However, since the south of Iceland is an α -ocean, these recent changes have
396 not yet reached or affected the MLD.

397 The northwestern region, which includes the Denmark Strait, is a medley of all the water masses described in this study.
398 In this region there is a confluence of Greenland shelf and slope waters and Iceland Sea origin waters (Harden et al., 2016;
399 Foukal et al., 2020). This includes the NIIC generating an important variability in the water properties due to complex
400 interactions of the regional currents (Lin et al. 2020, Mastropole et al. 2017). The MLD variability over time at the KG6
401 and LB8 stations is moderate (<100m), except for the years 2000, 2007 and 2016 when the ML was anomalously deep. In
402 this region, the stratification is notably year-round dominated by salinity (β -ocean), which is explained by the strong Polar
403 influence of cold and fresh waters transported by the EGC. A broader look into the northwestern side of the basin reveals
404 that this area can be divided at the center of the Denmark Strait into an α -ocean near the Icelandic shelf where the NIIC
405 flows and a β -ocean as we progress towards Greenland (where the LB8 and KG6 stations are located). Near the Icelandic
406 shelf, MLDs are driven mainly by wind-stress, with a secondary contribution of heat fluxes. The T-S properties as well as
407 the MLT anomalies in the northwest region near the Icelandic shelf show that the NIIC waters there are getting warmer and
408 saltier. This agrees with previous studies showing the transformation of the NIIC also accompanied by an increase in its
409 transport with time (Casanova-Masjoan et al., 2020). Even if the α -ocean area is warming, it is not expanding
410 northwestward. Hence, the EGC is acting as a barrier bringing PSW in the area and maintaining the β -ocean state on the
411 northwesternmost side of the Strait. This β -ocean, where the MLD is shallow all year round has dynamical implications as
412 the strong shallow stratification inhibits baroclinic instability and eddy generation (de Marez et al., 2025).

413 Northeast of Iceland, the ML exhibits intrusions of SW in the winter, while AW is present during the summer. In this
414 region, the stratification changes from β - to α -ocean seasonally. The Kolbeinsey Ridge acts as a barrier where we find the
415 eastward penetration of the EIC bringing fresh waters (PSWw) from the East Greenland Current (Macrander et al., 2014;
416 Casanova-Masjoan et al., 2020). In summer, the NIIC expands northeastward, bringing AW into the area and changing the
417 stratification regime to α . Hence, the mixed layer waters show important seasonal variability. They range from maximum
418 temperature below 2 °C in winter to over 10 °C in summer. This is also the only region where a significant warming decadal
419 trend emerges over the interannual variability and progressively results in a stronger α -ocean. This agrees with the AW
420 warming observed in Casanova-Masjoan et al. (2020) and with the northward progression of AW named as 'Atlantification'
421 described by Polyakov et al. (2017). This shift to α -ocean or 'Atlantification' may lead to deeper ML's (Moore et al., 2015;
422 Våge et al., 2022), and the associated deeper convection may increase the potential of this area to contribute to the dense
423 flow carried by the NIJ (Semper et al. 2019).

424 The regionalization proposed in this work, based on hydrographic properties, matches the recently proposed distribution
425 of primary production around Iceland (Richardson and Bendtsen, 2021; Cerfonteyn et al., 2023), supporting the importance
426 of MLD properties for the primary production (Ólafsson, 2003). The induced alterations on primary production can lead to
427 ecosystem changes. For example, Iceland has witnessed a rapid increase in the population of mackerel, a relatively warm-
428 water fish, since 2006 (Asthórsson et al., 2012; Campana et al., 2020) starting from the southeast towards the north and
429 recently they have been reported almost all around the country. This migration is consistent with our observations of both,
430 the increase in surface temperatures, *i.e.*, northward shift of warmer isotherms over the Iceland Faroe Ridge (de Marez et
431 al., 2025), and the increase of temperatures within the ML in the same regions over the last decade, which may establish
432 new pathways for entire ecosystems.

433 The long time series investigated here revealed important interannual oscillations of the ML properties. Four main
434 features are to be highlighted: (i) We do not observe any linear trend in the MLD, which is rather subjected to strong
435 interannual variability (ii) Except for the southern stations, influenced by the subpolar gyre, the interannual variability was
436 not correlated with the NAO. For example, FX9 shows a significant negative of MLT with the NAO ($R=-0.41$ and p -value
437 < 0.03). (iii) The southern stations, FX9, SB5, and ST5, within the α -ocean region, show a clear decrease in ML density,
438 with statistically significant values and accounting for a total decrease during the 29-year period of -0.08 kg/m^3 . (iv) The
439 linear fit indicates significant (at 95%) warming trends in the MLT of most of the stations in winter, with the maximum
440 trend of $0.08 \text{ }^\circ\text{C/year}$ at SI8 resulting in approximately $2.2 \text{ }^\circ\text{C}$. This agrees with previous studies (Sarafanov, 2009) showing
441 that the northern part of the North Atlantic (south of Iceland) is strongly dominated by atmospheric interannual to decadal
442 variability, particularly, where AW is present. The exception here is the northeastern region of Iceland where we observe
443 a clear warming trend of the ML (2010-2020). (v) We observe an ‘Atlantification’ expressed as a northeastward progression
444 of the α -ocean state. This progression will highlight the role of the northeastern area of Iceland as a convective zone where
445 deep water could be formed and contribute to the NIJ.

446 AUTHOR CONTRIBUTIONS

447 Conceptualization, ARA, MDPH and EP; methodology, ARA, EP and MDPH; software, ARA and AP; formal analysis,
448 ARA, EP, TM, CdM and MDPH; investigation, ARA, EP and MDPH, AM; data acquisition, SRÓ and AM; data curation,
449 SRÓ and AM; writing—original draft preparation, ARA, EP and MDPH; writing—review and editing, SRÓ, AM and SJ,
450 TM; visualization, ARA and EP; project administration, SRÓ; funding acquisition, ARA and SRÓ. All authors have read
451 and agreed to the published version of the manuscript.

452 FUNDING

453 ARA and CdM have been supported by HM Queen Margrethe II’s and Vigdís Finnbogadóttir’s Interdisciplinary
454 Research Centre on Ocean, Climate and Society (ROCS) under grant no. 158-4223. Support for this work was also
455 provided by the European Union’s Horizon 2020 research and innovation programme under grant no. 727852, Blue-
456 Action project (AM and SJ). This work has been supported by the FAR-DWO (PID2020-114322RB100) project from the
457 Spanish Ministry of Research.

458 ACKNOWLEDGMENTS

459 We are grateful for the invaluable cooperation we have had with the crews of the Icelandic research vessels Bjarni
460 Sæmundsson and Árni Friðriksson and to the many people at the Marine Research Institute that have contributed to the

461 hydrographic observations over the years. ARA and MDPH would like to dedicate this paper to the memory of Maria
462 Casanova-Masjoan.
463

464 **Table 2.** Characteristics for the representative stations for each typical surveyed section. The representative ocean currents
 465 at each section are also shown: North Icelandic Irminger Current (NIIC), Irminger Current (IC), East Greenland Current
 466 (EGC), North Icelandic Jet (NIJ), East Icelandic Current (EIC), and North Atlantic Current. (NAC). The corresponding
 467 stratification regimes are listed for summer and winter for each station.

468
 469

Station	Depth, [m]	Lon	Lat	Oceanic region	Significant currents	Stratification regime
Faxaflói (FX9)	1010	-27.98	64.35	Subpolar North Atlantic	IC	Alpha-ocean (summer) Weakly stratified (winter)
Látrabjarg (LB8)	658	-27.050	66.083	Denmark Strait	NIIC, EGC, DSO	Beta-ocean (all year round)
Kögur (KG6)	980	-23.933	67.583	Western Iceland Sea	EGC, DSO	Beta-ocean (all year round)
Síglunes (SI8)	1023	-18.83	68.00	Kolbeinsey Ridge	NIIC, EGC, EIC, NIJ	Transition (summer) Beta-ocean (winter)
Langanes NE (LN6)	1850	-12.66	68.00	Iceland Sea	EIC	Alpha-ocean (summer) Beta-ocean (winter)
Langanes E (LA8)	1251	-9.00	66.37	Iceland Sea	EIC	Alpha-ocean (summer) Transition (winter)
Krossanes (KR6)	1419	-9.00	65.00	Iceland Sea/ North Atlantic	EIC, NAC	Alpha-ocean (summer) Transition (winter)
Stokksnes (ST5)	1153	-13.66	63.66	North Atlantic	NAC	Alpha-ocean (summer) Weakly stratified (winter)
Selvogsbanki (SB5)	1006	-21.48	62.98	North Atlantic	IC	Alpha-ocean (summer) Weakly stratified (winter)

470
 471
 472
 473

Table 3. Main water masses definitions for the region of study (Rudels et al., 2005; Våge et al., 2011)

Water mass	Potential Temperature (θ)	Salinity	Potential density (σ_0 , kg m^{-3})
Surface Water (SW)	$> 3^\circ\text{C}$	-	$\sigma_0 < 27.70$
Warm Polar Surface Water (PSW _w)	$0^\circ\text{C} \leq \theta < 3^\circ\text{C}$	-	$\sigma_0 < 27$
Polar Surface Water (PSW)	$< 0^\circ\text{C}$,	-	$\sigma_0 < 27.70$

Atlantic Water(AW)	$> 3^{\circ}C$	> 34.9	-
Atlantic-origin Overflow Water (AtOW)	$0^{\circ}C \leq \theta < 3^{\circ}C$	-	$\sigma_0 \geq 27.8,$ $\sigma_{0.5} < 30.44$
Polar intermediate Water (PIW)	$0^{\circ}C$	≤ 34.676	$\sigma_0 > 27.70,$
Arctic-origin Overflow Water (ArOW)	$< 0^{\circ}C$	-	$\sigma_0 > 27.8,$ $\sigma_{0.5} < 30.44$
Nordic Seas Deep Water (NDW)	$< 0^{\circ}C$	-	$\sigma_{0.5} \geq 30.44$

474
475
476
477
478
479
480
481
482
483
484
485
486
487
488
489
490
491
492
493
494

495

497 **References**

- 498 Astthorsson, O. S., Valdimarsson, H., Gudmundsdottir, A., and Oskarsson, G. J.: Climate-related variations in the
 499 occurrence and distribution of mackerel (*Scomber scombrus*) in Icelandic waters, *ICES J. Mar. Sci.*, 69, 1289–1297, 2012.
- 500 Athanase, M., Provost, C., Perez-Hernández, M. D., Sennechael, N., Bertosio, C., Artana, C., et al.: Atlantic water
 501 modification north of Svalbard in the Mercator physical system from 2007 to 2020, *J. Geophys. Res.: Oceans*, 125,
 502 e2020JC016463, <https://doi.org/10.1029/2020JC016463>, 2020.
- 503 Bachman, S. D., Taylor, J., Adams, K., and Hosegood, P.: Mesoscale and submesoscale effects on mixed layer depth in
 504 the Southern Ocean, *J. Phys. Oceanogr.*, 47, 2173–2188, 2017.
- 505 Bindoff, N. L., Cheung, W. W., Kairo, J. G., Arístegui, J., Guinder, V. A., Hallberg, R., et al.: Changing ocean, marine
 506 ecosystems, and dependent communities, IPCC Special Report on the Ocean and Cryosphere in a Changing Climate, 477–
 507 587, 2019.
- 508 Brakstad, A.: Hydrographic and Geochemical Observations in the Nordic Seas Between 1950 and 2019, University of
 509 Bergen, 2023b.
- 510 Bersch, M.: North Atlantic Oscillation–induced changes of the upper layer circulation in the northern North Atlantic Ocean,
 511 *J. Geophys. Res.*, 107(C10), 3156, <https://doi.org/10.1029/2001JC000901>, 2002.
- 512 Campana, S. E., Stefansdottir, R. B., Jakobsdottir, K., and Solmundsson, J.: Shifting fish distributions in warming sub-
 513 Arctic oceans, *Sci. Rep.*, 10, 1–14, 2020.
- 514 Carmack, E. C.: The alpha/beta ocean distinction: A perspective on freshwater fluxes, convection, nutrients and
 515 productivity in high-latitude seas, *Deep Sea Res. Part II: Top. Stud. Oceanogr.*, 54, 2578–2598, 2007.
- 516 Carton, J. A., Grodsky, S. A., and Liu, H.: Variability of the oceanic mixed layer, 1960–2004, *J. Climate*, 21, 1029–1047,
 517 2008.
- 518 Casanova-Masjoan, M., Perez-Hernández, M. D., Pickart, R. S., Valdimarsson, H., Ólafsdóttir, S., Macrander, A., et al.:
 519 Along-stream, seasonal, and interannual variability of the North Icelandic Irminger Current and East Icelandic Current
 520 around Iceland, *J. Geophys. Res.: Oceans*, 125, e2020JC016283, <https://doi.org/10.1029/2020JC016283>, 2020.
- 521 Cerfonteyn, M., Groben, R., Vaulot, D., et al.: The distribution and diversity of eukaryotic phytoplankton in the Icelandic
 522 marine environment, *Sci. Rep.*, 13, 8519, <https://doi.org/10.1038/s41598-023-35516-w>, 2023.
- 523 Dai, A., Luo, D., Song, M., and Liu, J.: Arctic amplification is caused by sea-ice loss under increasing CO₂, *Nat. Commun.*,
 524 10, 1–13, 2019.
- 525 de Boyer Montégut, C., Madec, G., Fischer, A. S., Lazar, A., and Iudicone, D.: Mixed layer depth over the global ocean:
 526 An examination of profile data and a profile-based climatology, *J. Geophys. Res.: Oceans*, 109,
 527 <https://doi.org/10.1029/2004JC002378>, 2004.
- 528 de Marez, C., Ruiz-Angulo, A., & Gula, J. Mesoscale induced vertical fluxes over the Iceland-Faroe ridge. *Geophysical*
 529 *Research Letters*, 52(13), 2025.
- 530 de Marez, Charly, Clara R. Vives, Esther Portela, and Angel Ruiz-Angulo. Mesoscale ocean processes: The critical role
 531 of stratification in the Icelandic region. *Journal of Geophysical Research: Oceans* 130, no. 6 (2025).
- 532 Feucher, C., Portela, E., Kolodziejczyk, N., & Thierry, V. Subpolar gyre decadal variability explains the recent

533 oxygenation in the Irminger Sea. *Communications Earth & Environment*, 3(1), 279, 2022.

534 Foukal, N. P., Gelderloos, R., and Pickart, R. S.: A continuous pathway for fresh water along the east Greenland shelf, *Sci.*
535 *Adv.*, 6, eabc4254, 2020.

536 Fox-Kemper, B., H.T. Hewitt, C. Xiao, G. Aðalgeirsdóttir, S.S. Drijfhout, T.L. Edwards, N.R. Golledge, M. Hemer, R.E.
537 Kopp, G. Krinner, A. Mix, D. Notz, S. Nowicki, I.S. Nurhati, L. Ruiz, J.-B. Sallée, A.B.A. Slangen, and Y. Yu, 2021:
538 Ocean, Cryosphere and Sea Level Change. In *Climate Change 2021: The Physical Science Basis. Contribution of Working*
539 *Group I to the Sixth Assessment Report of the Intergovernmental Panel on Climate Change* [Masson-Delmotte, V., P. Zhai,
540 A. Pirani, S.L. Connors, C. Péan, S. Berger, N. Caud, Y. Chen, L. Goldfarb, M.I. Gomis, M. Huang, K. Leitzell, E. Lonnoy,
541 J.B.R. Matthews, T.K. Maycock, T. Waterfield, O. Yelekçi, R. Yu, and B. Zhou (eds.)]. Cambridge University Press,
542 Cambridge, United Kingdom and New York, NY, USA, pp. 1211–1362, doi: 10.1017/9781009157896.011.

543 Gjelstrup CVB, Sejr MK, de Steur L, Christiansen JS, Granskog MA, Koch BP, Møller EF, Winding MHS, Stedmon CA.
544 2022. Vertical redistribution of principle water masses on the northeast Greenland Shelf. *Nature Communications* 13:
545 doi:10.1038/s41 467–022–35 413–z.

546 Hafrannsóknastofnun: Makrill *Scomber scombrus* Stofnmatskýrslur (stock assessment report), Hafrannsóknastofnun,
547 2024, https://www.hafogvatn.is/static/extras/images/mackerel_2024_techreport_is.html.

548 Hansen, B., and Østerhus, S.: North Atlantic–Nordic Seas exchanges, *Prog. Oceanogr.*, 45, 109–208, 2000.

549 Harden, B., Renfrew, I., and Petersen, G.: Meteorological buoy observations from the central Iceland Sea, *J. Geophys.*
550 *Res.-Atmos.*, 120, 3199–3208, 2015.

551 Harden, B. E., Pickart, R. S., Valdimarsson, H., Vage, K., de Steur, L., Richards, C., et al.: Upstream sources of the
552 Denmark Strait overflow: Observations from a high-resolution mooring array, *Deep-Sea Res. Pt. I*, 112, 94–112, 2016.

553 Hátún, H., and Chafik, L.: On the recent ambiguity of the North Atlantic Subpolar Gyre Index, *J. Geophys. Res.-Oceans*,
554 123, 5072–5076, 2018.

555 Hátún, H., Chafik, L., and Larsen, K. M. H.: The Norwegian Sea Gyre – a regulator of Iceland-Scotland Ridge exchanges,
556 *Front. Mar. Sci.*, 8, 1001, 2021.

557 Havik, L., Pickart, R. S., Våge, K., Torres, D. J., Thurnherr, A., Beszczynska-Möller, A., et al.: Evolution of the East
558 Greenland Current from Fram Strait to Denmark Strait: Synoptic measurements from summer 2012, *J. Geophys. Res.-*
559 *Oceans*, 122, 1974–1994, 2017.

560 Hersbach, H., Bell, B., Berrisford, P., et al.: The ERA5 global reanalysis, *Q. J. R. Meteorol. Soc.*, 146, 1999–2049,
561 <https://doi.org/10.1002/qj.3803>, 2020.

562 Holt, J., Schrum, C., Cannaby, H., Daewel, U., Allen, I., Artioli, Y., et al.: Potential impacts of climate change on the
563 primary production of regional seas: A comparative analysis of five European seas, *Prog. Oceanogr.*, 140, 91–115, 2016.

564 Holte, J., Talley, L. D., Gilson, J., and Roemmich, D.: An Argo mixed layer climatology and database, *Geophys. Res. Lett.*,
565 44, 5618–5626, 2017.

566 Huang J, Pickart RS, Chen Z, Huang RX. 2023. Role of air-sea heat flux on the transformation of Atlantic Water encircling
567 the Nordic Seas. *Nature Communications* 14: doi:10.1038/s41 467–023–35 889–3.

568 Ingvaldsen, R. B., Assmann, K. M., Primicerio, R., Fossheim, M., Polyakov, I. V., and Dolgov, A. V.: Physical
569 manifestations and ecological implications of Arctic Atlantification, *Nat. Rev. Earth Environ.*, 2, 874–889, 2021.

- 570 Jónsson, S.: The circulation in the northern part of the Denmark Strait and its variability, *ICES CM*, 50, 1999.
- 571 Jónsson, S., and Briem, J.: Flow of Atlantic water west of Iceland and onto the North Icelandic shelf, 2003.
- 572 Jónsson, S., and Valdimarsson, H.: Water mass transport variability to the North Icelandic shelf, 1994–2010, *ICES J. Mar. Sci.*, 69, 809–815, <https://doi.org/10.1093/icesjms/fss024>, 2012.
- 573
- 574 Kohler, J., Serra, N., Bryan, F. O., Johnson, B. K., and Stammer, D.: Mechanisms of mixed-layer salinity seasonal variability in the Indian Ocean, *J. Geophys. Res.-Oceans*, 123, 466–496, 2018.
- 575
- 576 Li, G., Cheng, L., Zhu, J., Trenberth, K. E., Mann, M. E., and Abraham, J. P.: Increasing ocean stratification over the past half-century, *Nat. Clim. Chang.*, 10, 1116–1123, 2020.
- 577
- 578 Liu, C., Liang, X., Chambers, D. P., and Ponte, R. M.: Global patterns of spatial and temporal variability in salinity from multiple gridded Argo products, *J. Clim.*, 33, 8751–8766, 2020.
- 579
- 580 Logemann, K., Ólafsson, J., Snorrason, A., Valdimarsson, H., and Marteinsdóttir, G.: The circulation of Icelandic waters – a modelling study, *Ocean Sci.*, 9, 931–955, 2013.
- 581
- 582 Lozier, M. S., Li, F., Bacon, S., Bahr, F., Bower, A. S., Cunningham, S., et al.: A sea change in our view of overturning in the subpolar North Atlantic, *Science*, 363, 516–521, 2019.
- 583
- 584 Macrander, A., Valdimarsson, H., and Jonsson, S.: Improved transport estimate of the East Icelandic Current 2002–2012, *J. Geophys. Res.-Oceans*, 119, 3407–3424, 2014.
- 585
- 586 Mastropole, D., Pickart, R. S., Valdimarsson, H., Våge, K., Jochumsen, K., and Girton, J.: On the hydrography of Denmark Strait, *J. Geophys. Res.-Oceans*, 122, 306–321, 2017.
- 587
- 588 Mauritzen, C.: Production of dense overflow waters feeding the North Atlantic across the Greenland-Scotland Ridge. Part 1: Evidence for a revised circulation scheme, *Deep-Sea Res. Pt. I*, 43, 769–806, 1996.
- 589
- 590 Moore, G. W. K., Våge, K., Pickart, R. S., & Renfrew, I. A. (2015). Decreasing intensity of open-ocean convection in the Greenland and Iceland seas. *Nature Climate Change*, 5(9), 877-882.
- 591
- 592 Ólafsson, J.: Winter mixed layer nutrients in the Irminger and Iceland seas, *ICES Mar. Sci. Symp.*, 219, 329–332, 2003.
- 593
- 594 Intergovernmental Panel on Climate Change (IPCC): Special report on the ocean and cryosphere in a changing climate, 2019.
- 595
- 596 Ólafsdóttir, A. H., Utne, K. R., Jacobsen, J. A., Jansen, T., Óskarsson, G. J., Nøttestad, L., Elvarsson, B. Þ., Broms, C., and Slotte, A.: Geographical expansion of Northeast Atlantic mackerel (*Scomber scombrus*) in the Nordic Seas from 2007 to 2016 was primarily driven by stock size and constrained by low temperatures, *Deep-Sea Res. Pt. II*, 159, 152–168, 2019.
- 597
- 598 Østerhus, S., Woodgate, R., Valdimarsson, H., Turrell, B., De Steur, L., Quadfasel, D., Olsen, S. M., Moritz, M., Lee, C. M., Larsen, K. M. H., and Jónsson, S.: Arctic Mediterranean exchanges: a consistent volume budget and trends in transports from two decades of observations, *Ocean Sci.*, 15, 379–399, 2019.
- 599
- 600
- 601 Perez, F. F., Ólafsson, J., Olafsdóttir, S. R., Fontela, M., and Takahashi, T.: Contrasting drivers and trends of ocean acidification in the subarctic Atlantic, *Sci. Rep.*, 11, 1–16, 2021.
- 602
- 603 Perez-Hernández, M. D., Pickart, R. S., Torres, D. J., Bahr, F., Sundfjord, A., Ingvaldsen, R., et al.: Structure, transport, and seasonality of the Atlantic Water boundary current north of Svalbard: Results from a yearlong mooring array, *J. Geophys. Res.-Oceans*, 124, 1679–1698, 2019.
- 604
- 605
- 606 Petit, T., Lozier, M. S., Josey, S. A., and Cunningham, S. A.: Atlantic deep water formation occurs primarily in the Iceland

607 Basin and Irminger Sea by local buoyancy forcing, *Geophys. Res. Lett.*, 47, e2020GL091028, 2020.

608 Petit, T., Lozier, M. S., Josey, S. A., and Cunningham, S. A.: Role of air-sea fluxes and ocean surface density on the
609 production of deep waters in the eastern subpolar gyre of the North Atlantic, *Ocean Sci. Discuss.*, 1–21, 2021.

610 Piron, A., Thierry, V., Mercier, H., and Caniaux, G.: Argo float observations of basin-scale deep convection in the Irminger
611 Sea during winter 2011–2012, *Deep-Sea Res. Pt. I*, 109, 76–90, 2016.

612 Polyakov, I. V., Pnyushkov, A. V., Alkire, M. B., Ashik, I. M., Baumann, T. M., Carmack, E. C., et al.: Greater role for
613 Atlantic inflows on sea-ice loss in the Eurasian Basin of the Arctic Ocean, *Science*, 356, 285–291, 2017.

614 Polyakov, I. V., Rippeth, T. P., Fer, I., Alkire, M. B., Baumann, T. M., Carmack, E. C., et al.: Weakening of cold halocline
615 layer exposes sea ice to oceanic heat in the eastern Arctic Ocean, *J. Clim.*, 33, 8107–8123, 2020.

616 Price, J. F., Weller, R. A., and Pinkel, R.: Diurnal cycling – Observations and models of the upper ocean response to diurnal
617 heating, cooling, and wind mixing, *J. Geophys. Res.-Oceans*, 91, 8411–8427, 1986.

618 Renfrew, I. A., Pickart, R. S., Våge, K., Moore, G. W., Bracegirdle, T. J., Elvidge, A. D., et al.: The Iceland Greenland
619 Seas Project, *Bull. Am. Meteorol. Soc.*, 100, 1795–1817, 2019.

620 Reynolds, R. and Banzon, V.: NOAA optimum interpolation 1/4 degree daily sea surface temperature (OISST) analysis,
621 version 2, NOAA Natl. Cent. Environ. Inf., 10, V5SQ8XB5, 2008.

622 Richardson, K. and Bendtsen, J.: Distinct seasonal primary production patterns in the sub-polar gyre and surrounding seas,
623 *Front. Mar. Sci.*, 2021.

624 Rudels, B., Björk, G., Nilsson, J., Winsor, P., Lake, I., and Nohr, C.: The interaction between waters from the Arctic Ocean
625 and the Nordic Seas north of Fram Strait and along the East Greenland Current: Results from the Arctic Ocean-02 Oden
626 expedition, *J. Mar. Syst.*, 55, 1–30, 2005.

627 Sallée, J.-B., Pellichero, V., Akhoudas, C., Pauthenet, E., Vignes, L., Schmidtke, S., et al.: Summertime increases in upper-
628 ocean stratification and mixed-layer depth, *Nature*, 591, 592–598, 2021.

629 Sarafanov, A.: On the effect of the North Atlantic Oscillation on temperature and salinity of the subpolar North Atlantic
630 intermediate and deep waters, *ICES J. Mar. Sci.*, 66, 1448–1454, 2009.

631 Sarmiento, J. L., Hughes, T. M., Stouffer, R. J., and Manabe, S.: Simulated response of the ocean carbon cycle to
632 anthropogenic climate warming, *Nature*, 393, 245–249, 1998.

633 Semper, S., Våge, K., Pickart, R. S., Valdimarsson, H., Torres, D. J., and Jónsson, S.: The emergence of the North Icelandic
634 Jet and its evolution from Northeast Iceland to Denmark Strait, *J. Phys. Oceanogr.*, 49, 2499–2521, 2019.

635 Shepherd, J. G., Brewer, P. G., Oschlies, A., and Watson, A. J.: Ocean ventilation and deoxygenation in a warming world:
636 Introduction and overview, 2017 [Dataset].

637 Skyllingstad, E. D., Samelson, R. M., Simmons, H., Laurent, L. S., Merrifield, S., Klenz, T., and Centurioni, L.: Boundary
638 layer energetics of rapid wind and wave forced mixing events, *J. Phys. Oceanogr.*, 53, 1887–1900, 2023.

639 Stewart, K. D. and Haine, T. W.: Thermobaricity in the transition zones between alpha and beta oceans, *J. Phys. Oceanogr.*,
640 46, 1805–1821, 2016.

641 Strehl, A.-M., Våge, K., Merdrud, S. L. H., and Barreyre, T.: A 70-year perspective on water-mass transformation in the
642 Greenland Sea: From thermobaric to thermal convection, *Prog. Oceanogr.*, 227, 103304, 2024.

643 Swift, J. H., Aagaard, K., and Malmberg, S.-A.: The contribution of the Denmark Strait overflow to the deep North Atlantic,

644 Deep-Sea Res. Pt. A, 27, 29–42, 1980.

645 Tesdal, J.-E., Abernathy, R. P., Goes, J. I., Gordon, A. L., and Haine, T. W.: Salinity trends within the upper layers of the
646 subpolar North Atlantic, *J. Clim.*, 31, 2675–2698, 2018.

647 Valdimarsson, H., Astthórsson, O. S., and Pálsson, J.: Hydrographic variability in Icelandic waters during recent decades
648 and related changes in distribution of some fish species, *ICES J. Mar. Sci.*, 69, 816–
649 825, <https://doi.org/10.1093/icesjms/fss027>, 2012.

650 Våge, K., Moore, G. W. K., Jónsson, S., and Valdimarsson, H.: Water mass transformation in the Iceland Sea, *Deep-Sea*
651 *Res. Pt. I*, 101, 98–109, 2015.

652 Våge, K., Papritz, L., Havik, L., Spall, M. A., and Moore, G. W. K.: Ocean convection linked to the recent ice edge retreat
653 along East Greenland, *Nat. Commun.*, 9, 1–8, 2018.

654 Våge, K., Pickart, R. S., Moore, G., and Ribergaard, M. H.: Winter mixed layer development in the central Irminger Sea:
655 The effect of strong, intermittent wind events, *J. Phys. Oceanogr.*, 38, 541–565, 2008.

656 Våge, K., Pickart, R. S., Spall, M. A., Moore, G., Valdimarsson, H., Torres, D. J., et al.: Revised circulation scheme north
657 of the Denmark Strait, *Deep-Sea Res. Pt. I*, 79, 20–39, 2013.

658 Våge, K., Pickart, R. S., Spall, M. A., Valdimarsson, H., Jónsson, S., Torres, D. J., et al.: Significant role of the North
659 Icelandic Jet in the formation of Denmark Strait Overflow Water, *Nat. Geosci.*, 4, 723–727, 2011.

660 Våge, K., Semper, S., Valdimarsson, H., Jónsson, S., Pickart, R. S., & Moore, G. W. K. (2022). Water mass transformation
661 in the Iceland Sea: Contrasting two winters separated by four decades. *Deep Sea Research Part I: Oceanographic Research*
662 *Papers*, 186, 103824.

663 Whitney, M. M. (2025). Icelandic riverine freshwater distribution, offshore export, and alongshelf connectivity. *Estuarine,*
664 *Coastal and Shelf Science*, 319, 109266.

665 Yamaguchi, R. and Suga, T.: Trend and variability in global upper-ocean stratification since the 1960s, *J. Geophys. Res.-*
666 *Oceans*, 124, 8933–8948, 2019.

667

668